NJC

PAPER

View Article Online
View Journal | View Issue

Cite this: *New J. Chem.*, 2018, **42**, 14290

The photophysicochemical behavior of symmetric and asymmetric zinc phthalocyanines, surface assembled onto gold nanotriangles†

Edith Dube, Njemuwa Nwaji, John Mack and Tebello Nyokong *

Received 2nd June 2018,
Accepted 25th July 2018

DOI: 10.1039/c8nj02746c

rsc.li/njc

The synthesis of a novel asymmetric phthalocyanine, (4-(4-(benzo[*d*]thiazol-2-yl)phenoxy)-2,10,17-tris(4-(2-carboxyethyl)phenoxy)phthalocyaninatol)zinc(II), complex **3**, is reported. Complex **3** together with the previously reported complexes tetrakis[(benzo[*d*]thiazol-2-yl phenoxy)phthalocyaninato]zinc(II) (**4**) and 3-(4-((3,17,23-tris(4-(benzo[*d*]thiazol-2-yl)phenoxy)phthalocyaninatol)oxy)phenyl)propanoic acid zinc(II) (**5**), were linked to gold nanotriangles (AuNTs) through S–Au/Au–N self-assembly to afford the conjugates (**3**-AuNTs, **4**-AuNTs and **5**-AuNTs). The photophysicochemical behaviour of the complexes and their conjugates were studied. The asymmetric complexes **3** and **5**, displayed improved triplet and singlet oxygen quantum yields compared to the symmetric complex **4**, while all conjugates displayed improved triplet and singlet oxygen quantum yields compared to their respective complexes alone. The complexes and their conjugates could serve as good candidates for photodynamic therapy.

Introduction

Research on phthalocyanines (Pcs) for a variety of applications[1–6] is on the increase. Pcs are well known photosensitizers (PSs) for photodynamic therapy (PDT),[3,5,7,8] photodynamic antimicrobial therapy (PACT),[6] and the photodegradation of pollutants.[9] The applicability of Pcs as PSs emanates from their ability to absorb visible light, which excites them to an excited singlet state, followed by intersystem crossing to the excited triplet state. The triplet state then reacts with ground state molecular oxygen *via* energy transfer to form reactive oxygen species (including singlet oxygen) that can destroy cancer cells and pathogenic microbes.[6,10] The incorporation of heavy atoms in the central cavity of these Pcs to give metallophthalocyanines (MPcs) improves triplet state quantum yields through the heavy atom effect which promotes intersystem crossing to the triplet manifold.[11] However, the lack of selective accumulation of MPcs into cancer cells is a major challenge in PDT.[7,8] As a result, MPcs are now linked to nanocarriers for improved targeting of tumors through the enhanced permeability and retention (EPR) effect, a phenomenon by which molecules of certain sizes tend to accumulate and be retained in solid tumor tissues selectively but not in normal tissue because of the leaky vasculature in a tumorous tissue.[12,13]

Gold nanoparticles (AuNPs) play an important role in the biomedical fields especially in PDT as nanocarriers. The marked interest in AuNPs emanates from the unique chemical and physical properties that enable them to transport and deliver drugs (such as MPcs).[14,15] Ease of synthesis and functionalization, biocompatibility, inertness and non-toxicity makes AuNPs attractive nanocarriers.[16] They also exhibit size and shape dependent electronic and chemical properties.[17] Gold nanostars,[18] nanospheres,[19] nanorods and bipyramids[20] have been linked to phthalocyanines resulting in improved triplet state and singlet oxygen quantum yields. Gold nanotriangles (AuNTs) on the other hand, have been synthesized for photothermal therapy,[21] catalysis and for vapour sensing,[22] but have never previously been linked to Pcs. The ability of gold nanotriangles to generate singlet oxygen ($^1O_2$) was recently reported.[21] However, the probable enhancement in $^1O_2$ generation when these nanoparticles are formulated with phthalocyanines to form a nanohybrid has never been investigated. The efficiency of cellular uptake of the gold nanoparticles was found to rank in the following order: triangles > rods > stars.[23] Hence, AuNTs are employed in this work and are linked to MPcs for the first time.

The photophysical properties of a series of peripherally substituted ZnPc complexes **3–5** (Scheme 1) are compared when alone or linked to AuNTs. The Zn(II) ion is used in the central cavity of the three Pcs to promote rapid intersystem crossing to the triplet state through the heavy atom effect. Benzothiazole derivatives, have been found to have antitumor activities,[24] while ZnPc substituted with benzothiazole show improved

Centre for Nanotechnology Innovation, Department of Chemistry, Rhodes University, Grahamstown 6140, South Africa. E-mail: t.nyokong@ru.ac.za; Fax: +27 46 6225109; Tel: +27 46 6038260

† Electronic supplementary information (ESI) available: ^{1}H NMR, UV-visible absorption and MCD spectra, DFT and TD-DFT calculations, XPS and EDX spectra. See DOI: 10.1039/c8nj02746c

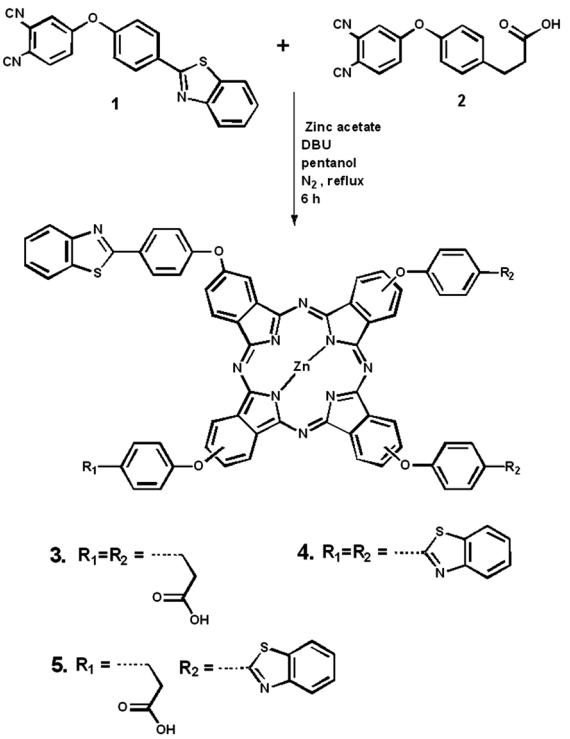

Scheme 1 Synthetic pathway for complex **3** and the structures of complexes **4** and **5**.

photophysical behavior.[25,26] We compare the effect of the peripheral benzothiazole groups by comparing the previously reported complex **4**[26] (four benzothiazoles), with **5** (three benzothiazoles) and **3** (one benzothiazoles). We also compare **5** (one propanoic acid), which has been reported previously,[27] with complex **3** (three propanoic acids). Porphyrins containing propanoic acid groups (such as the uroporphyrins) have been employed successfully for PDT.[10] **3** and **5** are asymmetrical (Scheme 1). Asymmetry is known to introduce distortion on the phthalocyanine macrocycle which affects the electronic states of the conjugated macrocycle ring, hence the photophysical properties of the Pc.[28] Complexes **3**, **4** and **5**, were linked to AuNTs *via* Au–S/Au–N self-assembly.

Experimental

Materials

Ultra-pure water was obtained from a Milli-Q Water System (Millipore Corp, Bedford, MA, USA), zinc(II) acetate dihydrate, 1-pentanol, 1,8-diazobicyclo[5.4.0]undec-7-ene (DBU), zinc phthalocyanine (ZnPc), 1,3-diphenylisobenzofuran (DPBF) and anthracene-9,10-bis-methylmalonate (ADMA) were purchased from Sigma-Aldrich. Tetrahydrofuran (THF), *N*,*N*-dimethyl formamide (DMF) and dimethyl sulphoxide (DMSO) were purchased from Merck. Methanol and absolute ethanol were obtained from Saarchem. All other reagents and solvents were obtained from commercial suppliers and used as received. Silica gel 60 (0.063–0.200 mm) for column chromatography was used for the purification processes. $AlPcS_{mix}$ (a mixture of sulfonated derivatives) was used as a standard for singlet oxygen quantum yields determination in aqueous media, and was synthesized according to literature methods.[29] The syntheses of 4-(4-(benzothiazol-2-yl)phenoxy)phthalonitrile (complex **1**),[26] 3(4-(phenoxy)-propanoic acid)phthalonitrile (complex **2**),[19] and gold nanotriangles (AuNTs),[30] have been reported previously in the literature.

Equipment

Ground state electronic absorption spectra were measured using a Shimadzu UV-2550 spectrophotometer. Mass spectra data were collected on a Bruker AutoFLEX III Smart-beam TOF/TOF mass spectrometer using α-cyano-4-hydrocinnamic acid as the matrix. Infrared spectra were acquired on a Bruker ALPHA FT-IR spectrometer with universal attenuated total reflectance (ATR) sampling accessory. ^{1}H NMR spectra were recorded on Bruker AVANCE II 600 MHz NMR spectrometers using tetramethylsilane (TMS) as an internal reference. Elemental analyses were performed using a Vario-Elementar Microcube ELIII. Fluorescence excitation and emission spectra were measured on a Varian Eclipse spectrofluorimeter using a 360–1100 nm filter. Excitation spectra were recorded using the Q-band maximum of the emission spectra as the excitation wavelength.

Fluorescence lifetimes were measured using a time-correlated single photon counting setup (TCSPC) (FluoTime 300, Picoquant GmbH) with a diode laser (LDH-P-670, Picoquant GmbH, 20 MHz repetition rate, 44 ps pulse width). Fluorescence was detected under the magic angle with a Peltier cooled photomultiplier tube (PMT) (PMA-C 192-N-M, Picoquant) and integrated electronics (PicoHarp 300E, Picoquant GmbH). A monochromator with a spectral width of *ca.* 8 nm was used to select the required emission wavelength band. The response function of the system, which was measured with a scattering Ludox solution (DuPont), had a full width at half-maximum (FWHM) of about 300 ps. The ratio of stop to start pulses was kept low (below 0.05) to ensure good statistics. All luminescence decay curves were measured at the maximum of the emission peak. The data were analysed with the program FluoFit (Picoquant).

Triplet state quantum yields were determined using a laser flash photolysis system consisting of an LP980 spectrometer with a PMT-LP detector and an ICCD camera (Andor DH320T-25F03). The signal from a PMT detector was recorded on a Tektronix TDS3012C digital storage oscilloscope. The excitation pulses were produced using a tunable laser system consisting of an Nd:YAG laser (355 nm, 135 mJ/4–6 ns) pumping an optical parametric oscillator (OPO, 30 mJ/3–5 ns) with a wavelength range of 420–2300 nm (NT-342B, Ekspla).

Irradiations for singlet oxygen quantum yield determinations were performed using a general electric quartz lamp (300 W) as described in the literature.[31] Light intensity was measured with a POWER MAX 5100 (Molelectron Detector Incorporated) power meter and was found to be 4.3×10^{15} photons cm^{-2} s^{-1}.

X-ray powder diffraction patterns were recorded using a Cu K radiation (1.5405 Å, nickel filter), on a Bruker D8 Discover equipped with a proportional counter and the data was processed using the Eva (evaluation curve fitting) software. Transmission electron microscope (TEM), ZEISS LIBRA® model 120 operated

at 90 kV was used for the assessment of morphologies of the NPs and their conjugates. Elemental compositions of the NPs and the conjugates were qualitatively determined using energy dispersive X-ray spectroscopy (EDX), INCA PENTA FET coupled to the VAGA TESCAM operated at 20 kV accelerating voltage.

Syntheses

The synthesis of complexes **4** and **5** has been previously reported,[26,27] while **3** is reported for the first time.

Synthesis of tris[3-(4-(phenoxy)phenyl)propanoic acid)-4-(bezothiazol-2-ylphenoxylphthalocyaninato]zinc(II) (3) (Scheme 1). A mixture of 4-(4-(benzothiazol-2-yl)phenoxy)phthalonitrile (**1**) (0.11 g, 0.31 mmol), 3(4-(phenoxy)-propanoic acid)phthalonitrile (**2**) (0.46 g, 1.56 mmol) and zinc(II) acetate dihydrate (0.20 g, 0.96 mmol) was dissolved in dry 1-pentanol (4 mL), after which DBU (≈0.1 mL) was added. The reaction mixture was refluxed at 160 °C for 6 h, under argon atmosphere. On cooling, methanol was added and the precipitate was collected under centrifugation. The precipitate was successively purified with methanol under centrifugation, dried and further purified by column chromatography using THF and methanol (90 : 10) as eluent, yielding complex **3**.

Yield: 0.08 g (14.0%). IR [ν_{max}/cm^{-1}]: 3065 (OH), 2921 (C–H stretch), 1719 (C=O), 1596, 1475 (C=C), 1230 (Ar–O–Ar). UV/Vis (DMSO), λ_{max} nm (log ε): 681 (4.85), 614 (4.16), 356 (4.48). ^{1}H NMR (600 MHz, DMSO-d_6) δ 11.32 (s, 3H, OH), 7.81 (d, J = 8.8 Hz, 2H, Ar-H), 7.37–7.09 (m, 30H, Ar-H), 2.89–2.85 (dd, J = 6.9, 1.5 Hz, 6H, CH_2), 2.68–2.65 (t, J = 5.7 Hz, 6H, CH_2), anal. calc. for ($C_{72}H_{47}N_9O_{10}SZn$): C, 66.74; H, 3.66; N, 9.73; S, 2.47. Found: C, 66.29: H, 3.89; N, 9.41; S, 3.00. MS (MALDI-TOF) m/z: calcd: 1295.64; found: 1295.40 [M]$^+$.

Linkage of complexes 3, 4 and 5 to AuNTs (Scheme 2). AuNTs (capped with hexadecyltrimethylammonium chloride, CTAC) were synthesized as reported in the literature.[30] The benzothiazole moieties of complexes **3**, **4** and **5**, containing sulphur and nitrogen groups are expected to form nitrogen–gold or sulphur–gold bonds with AuNTs through self-assembly mono layers. Complex **3** (0.02 g, 0.015 mmol), complex **4** (0.02 g, 0.0135 mmol) and complex **5** (0.02 g, 0.014 mmol) in DMF (4 mL) were each mixed with AuNTs (0.02 g) in water (2 mL), and left under stirring for 24 h at room temperature. The formed conjugates were washed with ethanol and collected by centrifugation. The conjugates are represented as **3**-AuNTs, **4**-AuNTs and **5**-AuNTs, where AuNTs stand for gold nanotriangles.

Photophysicochemical studies

Fluorescence (Φ_F) and triplet state (Φ_T) quantum yields of the complexes and conjugates were determined in DMSO using comparative methods described previously in the literature.[32–34] Unsubstituted ZnPc in DMSO was used as a standard with Φ_F = 0.20[33] and Φ_T = 0.65.[34] The solutions for triplet state studies were de-aerated with argon for 15 min before measurements. Singlet oxygen quantum yield (Φ_Δ) values were determined under ambient conditions using DPBF as a singlet oxygen scavenger in DMSO (and ADMA in water containing 0.5% DMSO) and calculated using equations that have been described previously.[35,36]

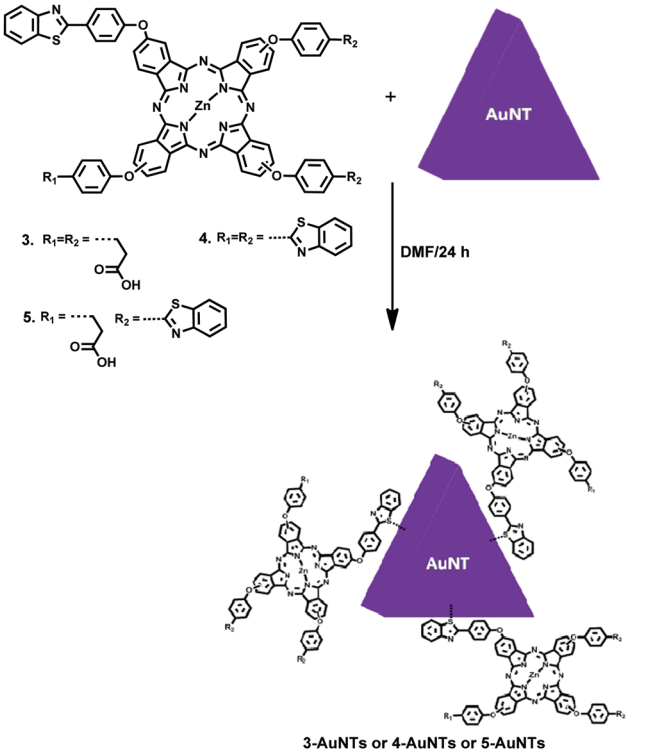

Scheme 2 Synthetic pathways for **3**-AuNTs, **4**-AuNTs and **5**-AuNTs.

ZnPc in DMSO was used as a standard (Φ_Δ = 0.67 in DMSO).[35] $AlPcS_{mix}$ was employed as a standard in aqueous media (Φ_Δ = 0.42).[37] The absorbances of DPBF or ADMA were spectroscopically monitored at 417 nm or 380 nm, respectively, at regular predetermined time intervals.

Theoretical calculations

The Becke, 3-parameter, Lee–Yang–Parr (B3LYP) functional was used to carry out geometry optimization for the four-fold symmetrical positional isomers of **3–5** in Gaussian 09 software package with SDD basis sets.[38] TD-DFT calculations were carried out using the CAM-B3LYP functional with SDD basis sets, since this functional contains a long-range connection that provides more accurate results for transitions with significant charge transfer character.[39]

Results and discussion

In this work, we report for the first time the synthesis of a low symmetry ZnPc, (24-(4-(benzo[*d*]thiazol-2-yl)phenoxy)-2,10,17-tris(4-(2-carboxyethyl)phenoxy)phthalocyanine-29-yl)zinc(II), complex **3**, consisting of three phenoxy propanoic acid and one benzothiazole phenoxy moieties. The synthetic route for the synthesis of a novel unsymmetrical zinc(II) phthalocyanine, complex **3** together with structures of complexes **4**[26] and **5**,[27] which have been reported previously, are shown in Scheme 1.

Complex **3**, was synthesized through a statistical cross-condensation of 4-(4-(benzothiazol-2-yl)phenoxy)phthalonitrile

(**1**) and 3-(4-phenoxy)-propanoic acidphthalonitrile (**2**). The disappearance of the characteristic C≡N peak of the dinitriles at 2230 cm^{-1} in the FT-IR spectrum of complex **3** (Fig. 1) confirmed the conversion of the phthalonitriles to a phthalocyanine.

The ^{1}H NMR spectrum for complex **3** (Fig. S1, ESI†) exhibited aromatic ring proton peaks resonating between 7.81–7.09 ppm, the CH_2 protons of the propionic acid chain were observed between 2.89 ppm and 2.65 ppm, while the protons due to the hydroxyl groups of the carboxylic acid moiety were found at 11.32 ppm. Peak integration gave the expected total number of protons, confirming the relative purity of the complex. Mass spectral data (Fig. S2, ESI†) and elemental analyses agreed with the proposed structure in Scheme 1.

An overlay of the normalized absorption spectra of complexes **3**, **4** and **5** in DMSO are shown in Fig. S3, ESI.† All complexes displayed two strong absorption bands, typical of metallated phthalocyanines with D_{4h} symmetry and in the absence of aggregation.[40] The Q band maxima of the complexes are shown in Table 1, and the values are not too different.

Complexes **3**, **4** and **5** and their conjugates with AuNTs are not soluble in water, hence for studies in water they were first dissolved in 50 μL DMSO and then diluted with water to 10 mL (0.5% DMSO). The aqueous media is important for future biological applications. For application in both *in vitro* and *in vivo* studies, the drugs are usually dissolved in DMSO and then diluted with water to the final concentration, given that hydrophilic–lipophilic balance is needed for effective performance of drug in the cells. However, the final concentration of DMSO in the diluted drug should be less than 1% to avoid DMSO toxicity.[41] This is the reason why 0.5% DMSO was used in this work.

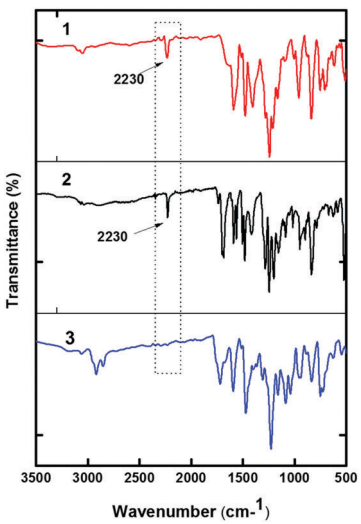

Fig. 1 FTIR spectra of complexes **1** to **3**.

Extensive aggregation was observed in aqueous media, Fig. S3B (ESI†). Aggregation in Pcs is judged by broad or split Q bands resulting from π–π stacking interaction of the aromatic rings of Pcs.[42] The effect of aggregation is usually reduced by solubilization of the drug in a biocompatible surfactant for therapeutic formulations.

MCD spectroscopy is another important technique for investigating the electronic structure of chromophores with high symmetry, such as porphyrins or phthalocyanines and provides essential information on their degenerate states.[43] The analysis of Faraday $\mathcal{A}_1$, $\mathcal{B}_0$ and $\mathcal{C}_0$ terms that form the basic principle of MCD spectroscopy provide information on the ground and excited state degeneracies. Although the MCD signal arises from the same transition that is responsible for the corresponding bands in the UV-visible absorption spectrum, the selection rules for the two techniques are different due to the use of circularly polarized light and an applied magnetic field in the context of MCD spectroscopy.

A distinctive S-shaped sigmoid curve was observed between 600 and 690 nm in the MCD spectra of **3–5** (Fig. 2 and Fig. S4, ESI†). The cross-over points between the upper and lower signal in the curve were found to be 681, 679 and 681 nm, for **3**, **4** and **5**, respectively, corresponding to absorption maxima of 681, 679 and 680 nm, for **3**, **4** and **5**, respectively, observed in the UV-vis spectra of **3–5** (Fig. 2 and Fig. S4, ESI†). It can, therefore, be assumed that the MCD spectrum in this spectral region is dominated by a pseudo-$\mathcal{A}_1$ term and hence the transition involves a near-degenerate excited state.[44] A similar curve was observed in the MCD spectrum at *ca.* 354, 345 and 355 nm for **3**, **4** and **5**, respectively. Thus, in accordance with Gouterman's 4-orbital model,[45] the Q band transitions can be readily assigned to the 681, 679 and 681 nm bands for **3**, **4** and **5**, respectively, and the B band transitions can in a similar way be assigned to the 359, 363 and 363 nm bands.

The optimized structures of complexes **3–5** showed a planar geometry with the metal lying inside the inner ring of the complexes (Fig. S5, ESI†). Single intense bands arising from the

Table 1 Photophysicochemical parameters of complexes **3**, **4**, and **5** and their conjugates in DMSO unless otherwise stated

Samples	Size (nm)	Pc loading[a] (μg mg^{-1})	λ_{abs}[b] (nm)	(Φ_F) (±0.01)	τ_F (ns) (±0.01)	(Φ_T) (±0.02) (DMSO)	T_T (μs) (±1.00)	Φ_Δ[c] (±0.01)
3		—	681	0.13	3.04	0.76	237	0.69 (0.14)
3-AuNTs	65.7	33	681 (638)	0.11	2.83	0.82	124	0.75 (0.16)
4		—	679	0.17	3.08	0.59	149	0.50 (0.07)
4-AuNTs	67.1	39	679 (638)	0.13	2.86	0.72	96	0.63 (0.11)
5		—	680	0.15	2.86	0.73	239	0.69 (0.15)
5-AuNTs	66.8	42	680 (638)	0.12	3.05	0.86	180	0.78 (0.19)

[a] Edge length in the conjugate, the edge length for AuNTs alone is 62.3 nm (from TEM). [b] Numbers in brackets are for the nanoparticles alone in water. [c] Numbers in brackets are the values in water containing 0.5% DMSO.

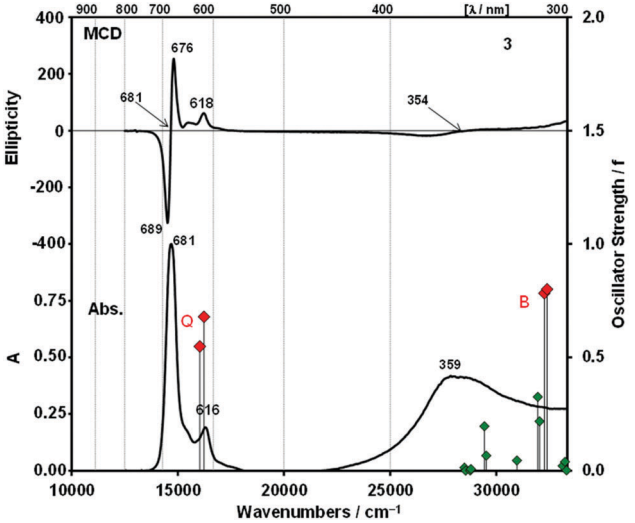

Fig. 2 Absorption and MCD spectra of **3** in DMSO. The calculated TD-DFT spectrum of the isomer of **3** is plotted against a secondary axis. Red diamonds are used to highlight bands associated with the Q and B bands of Gouterman's 4-orbital model. Details of the calculation are provided in Table S1, see ESI.†

Q and B transitions of Gouterman's orbital model are predicted in the TDDFT calculation for complexes **3–5** (Fig. 2 and Fig. S4, Table S1, ESI†). Peripheral substitution of the Pc ligand usually results in only a very minor splitting of the $1e_g^*$ LUMO (lowest unoccupied molecular orbital) of the parent unsubstituted ZnPc complex,[44] so it is reasonable to anticipate a single dominant pseudo-$\mathcal{A}_1$ term in Q and B band regions even in the context of asymmetrically-substituted complexes **3** and **5**. Many weaker transitions to other higher energy ππ* states are predicted to have similar energies to the B transition. This occurs as a broad envelope of overlapping bands in this spectral region.

An overlay of the absorption, excitation and emission spectra in DMSO are shown in Fig. 3 (using complex **3**, as an example). The ground state absorption and excitation spectra are mirror images of the emission spectrum. The closeness of the Q-band absorption and excitation maxima shows that the nuclear configurations of the ground and excited states are similar and are not affected by excitation in DMSO. It also shows that the complexes are not aggregated in DMSO.

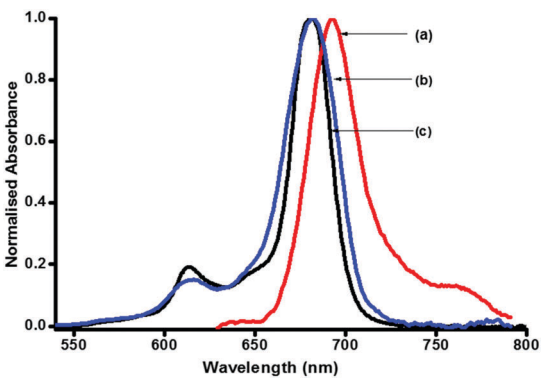

Fig. 3 Emission (a), excitation (b) and absorption (c) spectra of complex **3** (excitation = 610 nm, solvent = DMSO).

Characterization of AuNTs and conjugates

The normalised absorption spectra of AuNTs are shown in Fig. 4A. An intense band (dipole) around 638 nm and a weak shoulder (quadrupole) around 528 nm are observed, and these are attributed to the in-plane dipole and out-of-plane dipole resonance of gold nanoplates, respectively, characteristic of AuNTs.[46,47]

Conjugation of Pcs to AuNTs occurred by replacing loosely bound CTAC ligands with Au–S or Au–N bonds. The loading of complexes **3** to **5** onto the AuNTs was investigated following literature methods.[48] This involves dissolving the same mass of the Pc alone and the conjugate in an equal volume of solvent and comparing the Q band absorbance intensity of the Pc in the conjugate with that of the initial Pc before the conjugation. A decrease in intensity was observed in the conjugates compared Pc, due to adsorption of the Pc molecules onto the NP. The loadings of Pc onto nanoparticles are listed in Table 1.

The largest loading was for complex **5** (containing three benzothiazole substituents and one propanoic acid group) followed by complex **4**. Upon conjugation of complexes to AuNTs, an enhancement in absorption between the Q band and 500 nm was observed (Fig. 4B), which could be due to overlap of the absorption peak of the nanotriangles with the vibronic band of the complexes, hence confirming successful linkage of the

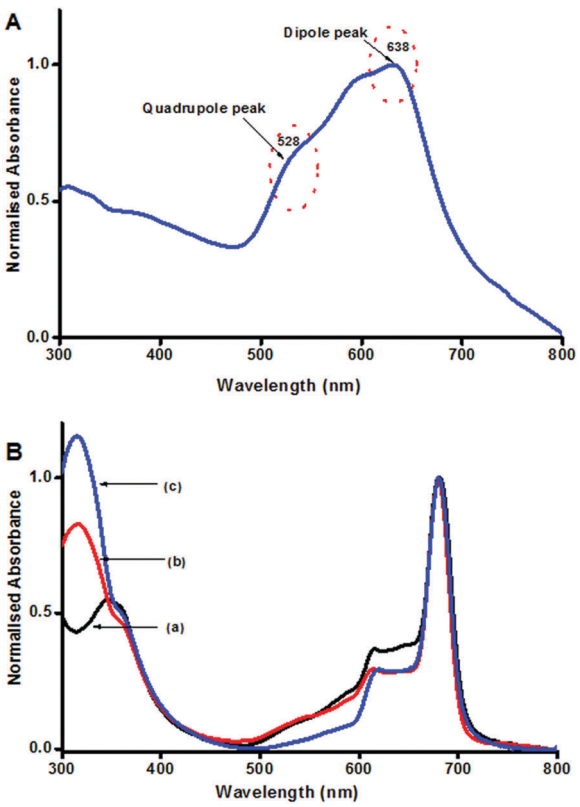

Fig. 4 UV-visible absorption spectra of (A) AuNTs in water and (B) **3**-AuNTs (a), **4**-AuNTs (b) and **5**-AuNTs (c) in DMSO.

complexes to nanoparticles. There was no change in the Q band absorption maxima of the complexes following conjugation, Table 1. In water (Fig. S3C, ESI†), aggregation discussed above continues for the conjugates.

Fig. 5 shows the powder XRD patterns for AuNTs, with **3**-AuNTs and complex **3** used as examples. The Pc complexes alone displayed broad peaks from 2θ = 10 to 32°, indicating the amorphous nature of phthalocyanines.[49] AuNTs together with the conjugates displayed sharp peaks at 2θ = 37.5, 44.3, 64.3, 76.9 and 80.8°, indicating their crystallinity, attributed to the presence of gold. These peaks were assigned to the 111, 200, 220, 311 and 222 planes, respectively, corresponding to the face centered-cubic structures of metallic gold.[50]

Fig. 6 shows the TEM micrographs of the AuNTs and the conjugates. The AuNTs image shows two different sizes of nanotriangles, at ~53 and ~78 nm (edge length), however average sizes are shown in Table 1. These two sizes could be responsible for the dipole peak at 638 nm (for larger size) and a shoulder peak at 600 nm (for smaller size) in the absorption spectrum of AuNTs, Fig. 4A. Also shown are a few irregular nanoparticles, pentagons and hexagons, which could be responsible for the quadrupole peak in Fig. 4A.[46]

Slight aggregation was observed for the nanotriangles before linkage to the complexes (Fig. 6), and it increased on linkage to the Pc complexes. Increased aggregation in the conjugates is likely due to π–π stacking that can occur between the Pcs and NPs. Pcs are known for their π–π stacking to form H aggregates.[42] The average sizes (edge lengths) of the NPs were estimated to be 62.3 nm for AuNTs, 65.7 nm for **3**-AuNTs, 67.1 nm for **4**-AuNTs and 66.8 nm for **5**-AuNTs.

An assessment of the possible interaction between AuNTs and complexes was done using XPS analysis, and complex **3** was used as an example. The XPS survey spectra exhibited the expected elements and their respective binding energies, Fig. S6, ESI.† Complex **3** exhibited S (157 eV), C (283 eV), N (395 eV), O (526 eV), and Zn (1017 eV). The peak around 100 eV in complex **3** could be due to residual silica during column chromatography. AuNTs exhibited Au (89 eV, 194 eV, 338 eV and 351 eV). The C and N peaks in the AuNTs are from the CTAC capping agent, which adsorbed on AuNTs. **3**-AuNTs, displayed similar atoms to both complex **3** and AuNTs. The energy dispersive X-ray spectrometer (EDX) (Fig. S7, ESI†), also confirmed the presence of the anticipated elements, however O was present in AuNTs, probably from the residual ascorbic acid used during synthesis.

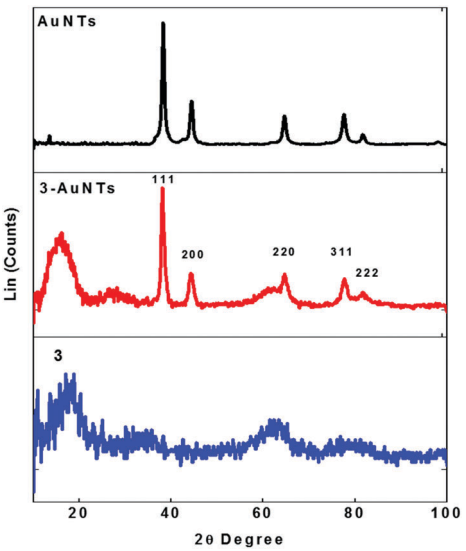

Fig. 5 XRD diffractograms for AuNTs, **3**-AuNTs, and complex **3**.

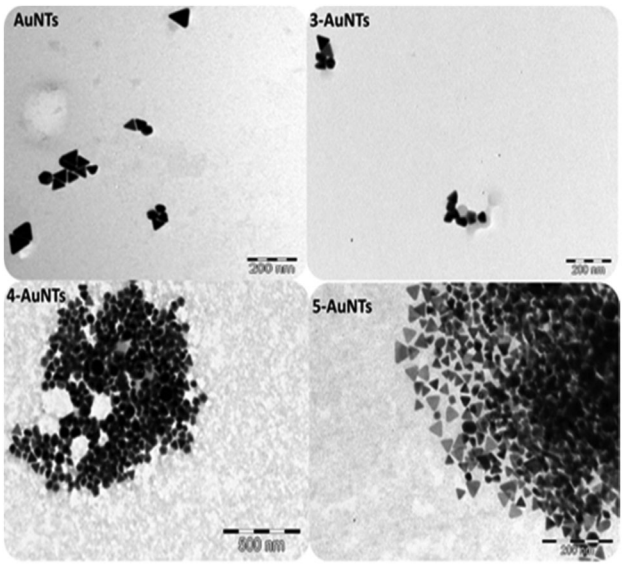

Fig. 6 Representative TEM micrographs for AuNTs, **3**-AuNTs, **4**-AuNTs and **5**-AuNTs.

To confirm linkage of complexes to AuNTs, the high resolution XPS analysis was employed. The S 2p deconvolution for complex **3** alone (Fig. 7A) exhibited two subpeaks corresponding to –S–C– (161.9 eV) and –S– (163.0 eV). The conjugates (Fig. 7B, **3**-AuNTs as an example) displayed three peaks attributed to –S–C– (161.8 eV), –S– (163.0 eV) and –S–Au– (166.7 eV). The N 1s peak for complex **3** alone (Fig. S6B, ESI†) showed two subpeaks corresponding to –N–C– (396.2 eV) and –N– (397.3 eV), while the conjugates (Fig. S6C ESI,† **3**–AuNTs as an example) displayed three peaks attributed to –N–C– (396.2 eV), –N– (397.5 eV) and –N–Au– (402.8 eV). The presence of both gold to sulfur and gold to nitrogen interaction (–N–Au– and –S–Au–) indicates that the complexes are linked to AuNTs through S–Au and N–Au interactions since gold has a strong affinity for both sulphur and nitrogen.

Photophysicochemical parameters

Table 1 shows the fluorescence quantum yields (Φ_F) and lifetimes (τ_F), triplet quantum yields (Φ_T) and lifetimes (τ_T), as well as singlet oxygen quantum yields (Φ_Δ) for **3**, **4** and **5** in DMSO before and after conjugation. The Φ_F and Φ_Δ values were also determined in water.

Fluorescence quantum yields (Φ_F) and lifetimes (τ_F)

In DMSO, the asymmetric complex **3** bearing three propanoic acid groups and one benzothiazole showed a lower fluorescence

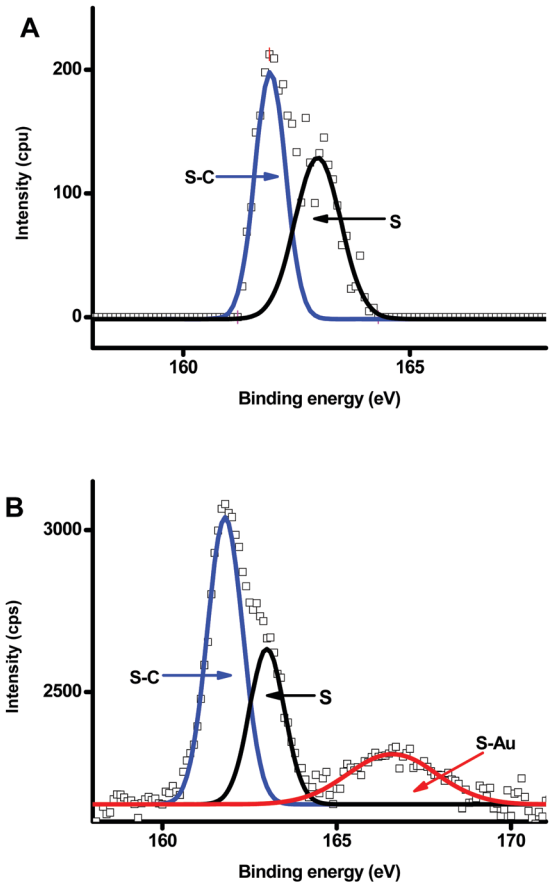

Fig. 7 XPS high resolution spectra (A) S 2p for complex **3** and (B) S 2p for **3**-AuNTs.

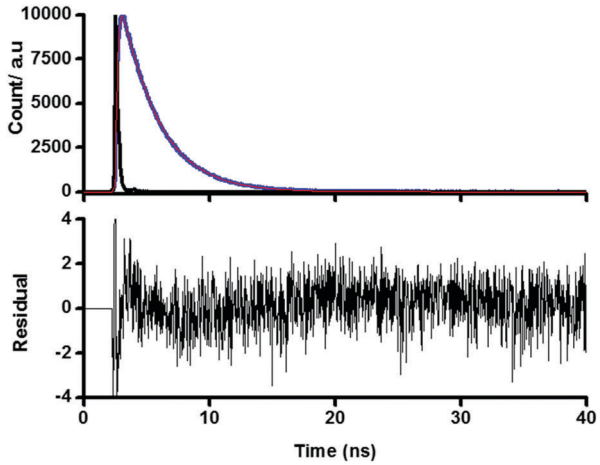

Fig. 8 Fluorescence decay (blue), χ^2 fitting (red) and IRF (black) curves for complex **4** in DMSO.

quantum yield of 0.13 as well as a lower lifetime of 3.04 ns compared to the quantum yield of 0.17 and lifetime of 3.08 ns for the symmetric complex **4** (containing only benzothiazole groups). This suggests that asymmetric structures could be potential means of enhancing intersystem crossing to the triplet state. The lifetimes of the complexes alone showed a mono-exponential decay, while the corresponding conjugates displayed bi-exponential decays, and hence there are two lifetime values (Fig. 8, using **4** as example). The average lifetimes for the conjugates are presented in Table 1. The presence of two lifetimes can be explained based either on the existence of aggregates, which quench fluorescence, resulting in shorter quenched and longer unquenched lifetimes[51] or on different orientations of the phthalocyanines on the NPs. Further deactivation of the excited singlet state was observed after the conjugation of the complexes to AuNTs, since Au is also a heavy atom.[52] The fluorescence lifetimes decreased upon conjugation with NPs since fluorescence quantum yields and lifetimes have a direct relationship, except for complex **5** and its conjugate with increased lifetimes after conjugation. The Φ_F values in water (containing 0.5% DMSO) were found to all be $<0.01\%$. The low Φ_F values in water are attributed to aggregation which usually quenches fluorescence. Aggregates are known to convert electronic excitation energy to vibrational energy which consequently decreases the fluorescence quantum yield of molecules.[53] The τ_F values in water could not be obtained probably due to very low fluorescence.

Triplet state quantum yields (Φ_T) and lifetimes (τ_T)

The triplet state quantum yield (Φ_T) represents the fraction of molecules that undergoes intersystem crossing to the triplet excited state. A high triplet state quantum yield with its corresponding low fluorescence quantum yield suggests that there is a more efficient intersystem crossing, which is an attractive feature for MPcs for use as photosensitizers. A high triplet quantum yield is of great importance since it influences the singlet oxygen production. Fig. 9B, shows the triplet decay curve of the conjugate **3**-AuNTs (as an example) together with its transient curve (Fig. 9A).

The transient absorption spectrum shows a broad band between 400–600 nm with a maximum at 505 nm, attributed to the triplet–triplet state excited absorption ($T_1 \rightarrow T_n$). The negative peaks were also shown between 325 and 380 nm and between 600 and 700 nm. Considering the shape and the position of the negative signals, which corresponds to the absorption in the ground state, these can be attributed to the depletion or photobleaching of the phthalocyanine ground state.[54]

The triplet decay curve obeyed second order kinetics, typical of MPc complexes at high concentration, due to triplet–triplet recombination.[55] The phthalocyanine complexes alone displayed high triplet quantum yield (Table 1) due to the presence of Zn with a heavy atom effect. In addition, the presence of carboxyl groups and sulphur atoms also favors intersystem crossing.[56] Due to the advantage of asymmetry, which introduces distortion thus lowering HOMO (highest occupied molecular orbital) to LUMO energy gap, asymmetric complexes **3** and **5** displayed higher Φ_T values compared to a symmetric complex **4**.

Complex **3**, with more carboxylic acid groups displayed a slightly higher Φ_T than complex **5**. Linkage of complexes to AuNTs further increased the triplet quantum yields (Table 1) due to the heavy atom effect of gold, as previously stated.

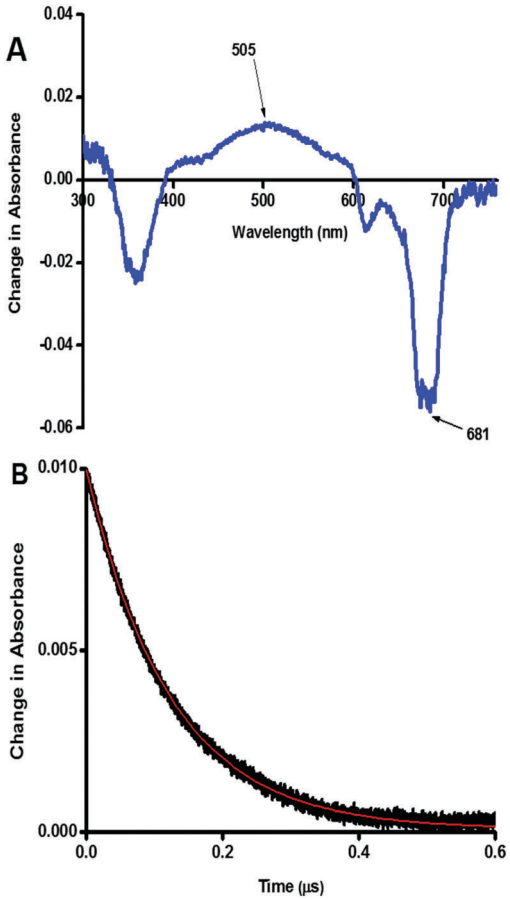

Fig. 9 (A) Transient curve and (B) triplet absorption decay curve (black) and fitting (red) for **3**-AuNTs in DMSO.

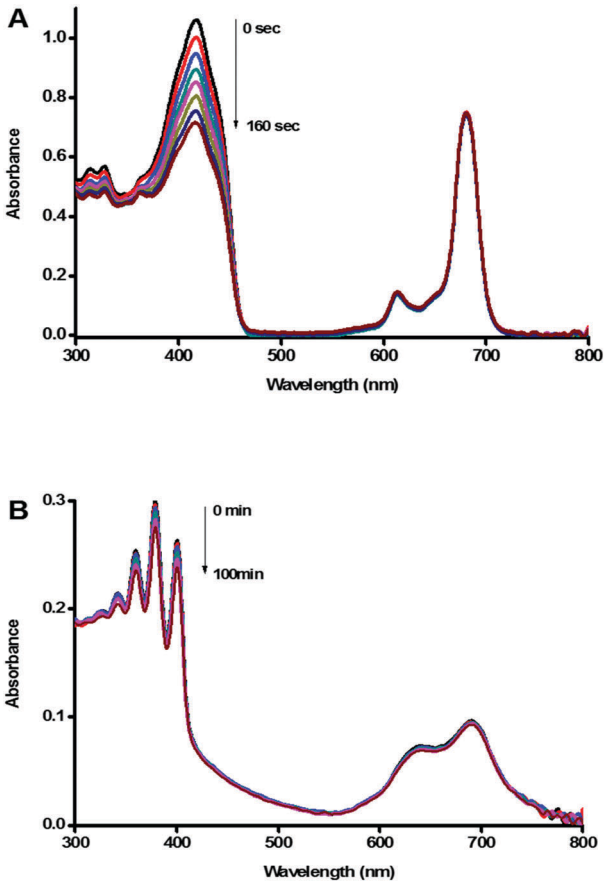

Fig. 10 Representative UV/Vis spectra for singlet oxygen quantum yield determination using a photochemical method. The spectra show the degradation of (A) DPBF in DMSO and (B) ADMA in water containing 0.5% DMSO in the presence of complex **3** and **4**, respectively.

On linkage of complexes to AuNTs, the conjugate **5**-AuNTs displayed a slightly higher Φ_T than **3**-AuNTs, even though the opposite was observed for complexes alone. This was attributed to the loading of more Pcs on the AuNTs for **5**-AuNTs than **3**-AuNTs, Table 1. The triplet lifetimes became shorter as the triplet quantum yields increased as expected.[57] Generally there were slight increases in Φ_T corresponding to slight decreases in Φ_F and this could probably be due to the distance or orientation between the MPc and the NTs. It has been shown that the distance between the fluorophore and the metallic nanoparticles affect their fluorescence properties.[58] The Φ_T value improves dramatically for the symmetrical complex **4** in the presence of AuNTs. This shows the symmetric MPc complexes, which have lower Φ_T values benefit more by linking to AuNTs. Due to the aggregation tendency of Pcs in aqueous media, the triplet quantum yields of the complexes and their conjugates could not be obtained.

Singlet oxygen quantum yields

The Φ_Δ value is the key indicator of the potential applicability of the complexes as photosensitizers. Values were determined through photodegradation with DPBF or ADMA as singlet oxygen scavengers in DMSO and aqueous media (Fig. 10).

The DPBF and ADMA degraded while the Q-band remained unchanged, proving the stability of the Pcs over the irradiation period. As expected, the Φ_Δ values (Table 1) followed the same trend observed for the Φ_T values, since singlet oxygen formation is dependent on the Φ_T value. The improvement in the Φ_Δ value is quite significant for the symmetrical derivatives corresponding to the improvement in triplet quantum yields. The values in water are lower due to aggregation since this reduces the excited state lifetimes and the photosensitizing efficiency, due to enhanced radiationless decay. Even though the values are low, the conjugates in this work can still be used for PDT since complexes such as lutetium texaphyrin with a low singlet oxygen value of 0.11 have been employed for clinical application in PDT.[10]

Conclusions

In this work, we report on the synthesis of novel (24-(4-(benzo[*d*]thiazol-2-yl)phenoxy)-2,10,17-tris(4-(2 carboxyethyl)-phenoxy)phthalocyanine-29-yl)zinc(II), complex **3**, which was characterised using FTIR, UV-Visible and ^{1}H NMR spectroscopy, MALDI-TOF mass spectrometry and elemental analyses. Complex **3** together with the previously reported complexes **4** and **5**, were linked to AuNTs through S–Au and Au–N self

assembly. The photophysicochemical behaviour of the complexes and their conjugates were studied. Asymmetric complexes **3** and **5**, displayed improved triplet state and singlet oxygen quantum yields compared to the symmetric complex **4**, while all the conjugates displayed improved triplet state and singlet oxygen quantum yields compared to complexes alone.

Conflicts of interest

There are no conflicts to declare.

Acknowledgements

This work was supported by the Department of Science and Technology (DST) Innovation and National Research Foundation (NRF), South Africa through DST/NRF South African Research Chairs Initiative for Professor of Medicinal Chemistry and Nanotechnology (UID 62620) as well as Rhodes University. Theoretical calculations were carried out at the Centre for High Performance Computing in Cape Town.

References

1 D. Wöhrle, G. Schnurpfeil, S. G. Makarov, A. Kazarin and O. N. Suvorova, *Macroheterocycles*, 2012, **5**, 191–202.
2 Y. Chen, M. Hanack, Y. Araki and O. Ito, *Chem. Soc. Rev.*, 2005, **34**, 517–529.
3 H. Ali and J. E. van Lier, *Chem. Rev.*, 1999, **99**, 2379.
4 E. Dube, D. O. Oluwole and T. Nyokong, *J. Lumin.*, 2017, **190**, 353–363.
5 M. Allen, W. M. Sharman and J. E. vanLier, *J. Porphyrins phthalocyanines*, 2001, **5**, 161.
6 M. Wainwright, *J. Antimicrob. Chemother.*, 1998, **42**, 13–28.
7 L. B. Josefsen and R. W. Boyle, *Theranostics*, 2012, **2**, 916–966.
8 J. Taquet, C. Frochot, V. Manneville and M. Barberi-Heyob, *Curr. Med. Chem.*, 2007, **14**, 1673–1687.
9 S. Mapukata, F. Chindeka, Ku. E. Sekhosana and T. Nyokong, *J. Mol. Catal. A: Chem.*, 2017, **439**, 211–223.
10 R. Bonnett, *Chemical aspects of photodynamic therapy*, Gordon and Breach Science Publishers, London, 2000.
11 K. N. Solov'ev and E. A. Borisevich, *Phys.-Usp.*, 2005, **48**, 231–253.
12 S. Kapse-Mistry, T. Govender, R. Srivastava and M. Yergeri, *Front. Pharmacol.*, 2014, **5**, 159.
13 Y. Omidi and J. Barar, *BioImpacts*, 2014, **4**, 55–67.
14 K. O. Shittu, M. T. Bankole, A. S. Abdulkareem, O. K. Abubakre and A. U. Ubaka, *Adv. Nat. Sci.: Nanosci. Nanotechnol.*, 2017, **8**, 035014.
15 F. K. Alanazi, A. A. Radwan and I. A. Alsarra, *Saudi Pharm. J.*, 2010, **18**, 179–193.
16 C. Kim, P. Ghosh and V. M. Rotello, *Nanoscale*, 2009, **1**, 61–67.
17 P. Chen, S. Mwakwari and A. Oyelere, *Nanotechnology*, 2008, **1**, 45–66.
18 S. D'Souza, S. Moeno, E. Antunes and T. Nyokong, *New J. Chem.*, 2013, **37**, 1950.
19 E. Dube, N. Nwaji, D. O. Oluwole, J. Mack and T. Nyokong, *J. Photochem. Photobiol., A*, 2017, **349**, 148–161.
20 T. Mthethwa and T. Nyokong, *J. Lumin.*, 2015, **157**, 207–214.
21 J. Lv, Y. Yi, G. Q. Wu and W. Liu, *Mater. Lett.*, 2017, **187**, 148–150.
22 B. Ankamwar, M. Chaudhary and M. Sastry, *Synth. React. Inorg., Met.-Org., Nano-Met. Chem.*, 2005, **35**, 19–26.
23 X. Xie, J. Liao, X. Shao, Q. Li and Y. Lin, *Sci. Rep.*, 2017, **7**, 3827.
24 E. E. Gurdal, E. Buclulgan, I. Durmaz, R. Cetin-Atalay and M. Yarim, *Anticancer Agents Med. Chem.*, 2015, **15**, 382–389.
25 N. Nwaji, O. M. Bankole, J. Britton and T. Nyokong, *J. Porphyrins phthalocyanines*, 2017, **21**, 263–272.
26 A. Aktaş, M. Durmuş and L. Değrmencioğlu, *Polyhedron*, 2012, **48**, 80–91.
27 E. Dube, D. O. Oluwole, E. Prinsloo and T. Nyokong, *New J. Chem.*, 2018, **42**, 10214–10225.
28 T. Fukuda, S. Homma and N. Kobayashi, *Chem. – Eur. J.*, 2005, **11**, 5205–5216.
29 M. Ambroz, A. Beeby, A. J. McRobert, M. S. C. Simpson, R. K. Svensen and D. Phillips, *J. Photochem. Photobiol., B*, 1999, **1**, 87.
30 L. Chen, F. Ji, Y. Xu, L. He, Y. Mi, F. Bao, B. Sun, X. Zhang and Q. Zhang, *Nano Lett.*, 2014, **14**, 7201–7206.
31 N. Masilela and T. Nyokong, *J. Photochem. Photobiol., A*, 2013, **255**, 1–9.
32 S. Fery-Forgues and D. Lavabre, *J. Chem. Educ.*, 1999, **76**, 1260–1264.
33 A. Ogunsipe, J. Y. Chen and T. Nyokong, *New J. Chem.*, 2004, **28**, 822–827.
34 T. H. Tran-Thi, C. Desforge, C. Thiec and S. J. Gaspard, *J. Phys. Chem.*, 1989, **93**, 1226–1233.
35 N. A. Kuznetsova, N. S. Gretsova, O. A. Yuzhakova, V. M. Negrimovskii, O. L. Kaliya and E. A. Luk'yanets, *Russ. J. Gen. Chem.*, 2001, **71**, 36–41.
36 W. Spiller, H. Kliesch, D. Wohrle, S. Hackbarth, B. Roder and G. Schnurpfeil, *J. Porphyrins phthalocyanines*, 1998, **2**, 145–158.
37 T. Nyokong and E. Antunes, Photochemical and photophysical properties of metallophthalocyanines, in *The Handbook of Porphyrin Science*, ed. K. M. Kadish, K. M. Smith and R. Guilard, World Scientific, Singapore, 2010, pp. 247–349.
38 M. J. Frisch, G. W. Trucks, H. B. Schlegel, G. E. Scuseria, M. A. Robb, J. R. Cheeseman, G. Scalmani, V. Barone, B. Mennucci, G. A. Petersson, H. Nakatsuji, M. Caricato, X. Li, H. P. Hratchian, A. F. Izmaylov, J. Bloino, G. Zheng, J. L. Sonnenberg, M. Hada, M. Ehara, K. Toyota, R. Fukuda, J. Hasegawa, M. Ishida, T. Nakajima, Y. Honda, O. Kitao, H. Nakai, T. Vreven, J. A. Montgomery, Jr., J. E. Peralta, F. Ogliaro, M. Bearpark, J. J. Heyd, E. Brothers, K. N. Kudin, V. N. Staroverov, R. Kobayashi, J. Normand, K. Raghavachari, A. Rendell, J. C. Burant, S. S. Iyengar, J. Tomasi, M. Cossi, N. Rega, J. M. Millam, M. Klene, J. E. Knox, J. B. Cross, V. Bakken, C. Adamo, J. Jaramillo, R. Gomperts, R. E. Stratmann, O. Yazyev, A. J. Austin, R. Cammi, C. Pomelli, J. W. Ochterski, R. L. Martin, K. Morokuma, V. G. Zakrzewski,

G. A. Voth, P. Salvador, S. Dannenberg, J. J. Dapprich, A. D. Daniels, Ö. Farkas, J. B. Foresman, J. V. Ortiz, J. Cioslowski and D. J. Fox, *Gaussian 09, Revision E.01*, Gaussian, 2009.
39 R. J. Magyar and S. Tretiak, *J. Chem. Theory Comput.*, 2007, **3**, 976–987.
40 I. Ozcesmeci, *Synth. Met.*, 2013, **176**, 128–133.
41 L. de, A. Costa, M. H. F. Ottoni, M. G. dos Santos, A. B. Meireles, V. G. de Almeida, Wa. de, F. Pereira, B. A. de Avelar-Freitas and G. E. A. Brito-Melo, *Molecules*, 2017, **22**, 1789.
42 M. J. Stillman and T. Nyokong, in *Phthalocyanines: Properties and applications*, ed. C. C. Leznoff and A. B. P. Lever, VCH Publishers, New York, 1989, ch. 3.
43 N. Kobayashi, A. Muranaka and J. Mack, *Circular Dichroism and Magnetic Circular Dichroism Spectroscopy for Organic Chemists*, Royal Society of Chemistry, London, 2011.
44 J. Mack and N. Kobayashi, *Chem. Rev.*, 2011, **111**, 281–321.
45 M. Gouterman, in *The Porphyrins*, ed. D. Dolphin, Academic Press, New York, 1978, vol. III, part A, pp. 1–165.
46 Z. Li, Yi. Yu, Z. Chen, T. Liu, Z. Zhou, J. Han, J. Li, C. Jin and X. Wang, *J. Phys. Chem. C*, 2013, **117**, 20127–20132.
47 J. E. Millstone, S. Park, K. L. Shuford, L. Qin, G. C. Schatz and C. A. Mirkin, *J. Am. Chem. Soc.*, 2005, **127**, 5312–5313.
48 L. Li, J. F. Zhao, N. Won, H. Jin, S. Kim and J. Y. Chen, *Nanoscale Res. Lett.*, 2012, **7**, 386–393.
49 R. Prabakaran, R. Kesavamoorthy, G. L. N. Reddy and F. P. Xavier, *Phys. Status Solidi*, 2002, **229**, 1175–1186.
50 A. M. H. Majles, Z. Dehghani, R. Sahraei, A. Daneshfar, Z. Javadi and F. Divsar, *J. Quant. Spectrosc. Radiat. Transfer*, 2012, **113**, 366–372.
51 Z. Petrásek and D. Phillips, *Photochem. Photobiol. Sci.*, 2003, **2**, 236–244.
52 Y. Shimzu and T. Azumi, *J. Phys. Chem.*, 1982, **86**, 22–26.
53 J. A. Lacey and D. Philips, *Photochem. Photobiol. Sci.*, 2002, **1**, 378–383.
54 Z. N. Erol, P. Atienzar, Y. Arslanoğlu, E. Hamuryudan and H. García, *RSC Adv.*, 2015, **5**, 55901.
55 M. G. Debacker, O. Deleplanque, B. Van Vlierberge and F. X. Sauvage, *Laser Chem.*, 1988, **8**, 1.
56 R. Mayildurai, G. Dhinakaran, S. Karthikeyan and R. Ashokkumar, *Rasayan J. Chem.*, 2017, **10**, 1242–1246.
57 J. R. Darwent, P. Douglas, A. Harriman, G. Porter and M. C. Richoux, *Coord. Chem. Rev.*, 1982, **44**, 83–126.
58 J. Kümmerlen, A. Leitner, H. Brunner, F. R. Aussenegg and A. Wokaun, *Mol. Phys.*, 1993, **80**, 1031–1046.